



IJSRM

INTERNATIONAL JOURNAL OF SCIENCE AND RESEARCH METHODOLOGY

An Official Publication of Human Journals




Human Journals

Research Article


November 2016 Vol.:5, Issue:1

© All rights are reserved by FATHY A. AMMAR et al.

Biotites from Sohail Island Granites, Aswan, Egypt: Chemistry, Structural Variations and Their Alteration to Chlorite



IJSRM
INTERNATIONAL JOURNAL OF SCIENCE AND RESEARCH METHODOLOGY
An Official Publication of Human Journals



AHMED M. BISHADY, FATHY A. AMMAR*

Geology department, Faculty of Science, Menoufiya University

**Nuclear Materials Authority of Egypt (ENMA)*

Submission: 5 November 2016
Accepted: 10 November 2016
Published: 25 November 2016



HUMAN JOURNALS

www.ijsrm.humanjournals.com

Keywords: Biotite, Chlorite, HRTEM, SAED, XRD, Sohail Island granite, Aswan, Egypt

ABSTRACT

Biotites and their intergrowths of chlorite from the Sohail Island granites have been studied through chemical analyses, powder X-ray diffraction (XRD), high-resolution transmission electron microscope (HRTEM) and selected area electron diffraction (SAED). The biotites are iron-enriched and crystallized between 710°C and 750°C. The chlorite intergrowths are represented mainly by chamosite (the brunsvigite variety), where the formation temperature of these chlorites is 272°C. The substantial alteration of biotite to chlorite takes place uncommonly by the replacement of TOT mica layers in the biotite by brucite-like layers, whereas the most common mechanism is that in which brucite like-layers grow into the interlayer planes of mica. XRD and microprobe analyses results of the biotite and chlorite proved volume changes through the processes of alteration. Volume discrepancies are re-equilibrated by the formation of porosity, micro-precipitates and/or change in rock volume by the adjustment of fractures. However, chlorite intergrowths were accompanied by the formation of micro-precipitates, possibly of quartz and/or amorphous silica on the planes of alteration. Very fine exsolutions of titanite and possibly magnetite can also represent some of these micro-precipitates. SAED and XRD patterns of the Sohail Island biotites indicate the common presence of the 1-M structure type, and probably some other polytypes. Mottling appears through HRTEM imaging among different biotite spacing.

INTRODUCTION

Biotite had been subjected to lot of studies exhibiting that they are commonly altered both chemically and texturally by subsolidus reactions of various types (Speer 1984, Zen 1988). Such post-magmatic reactions are mainly represented by the subsolidus replacement of biotite by chlorite and some other minerals (CHAYES 1955, FERRY 1979, BANIFIELD AND EGGLETON 1988, FERROW *ET AL.* 1990, KALINOWSKI AND SCHWEDA 1996).

The Aswan granitic rocks – including the Sohail Island granites – (Fig.1), were subjected to field, petrographic, geochemical and geochronological studies since 1907 (e.g. BALL 1907, HUME 1935, LITTLE AND ATTIA 1943, EL-SHAZLY 1954, ATTIA 1955, HUNTING 1967 AND OTHERS).

ABDEL-MONEM AND HURELY (1980) in their investigation of the age of Aswan monumental granite (Aswan granite) , suggested that the age of 700 Ma represents their age of formation, whereas the previously determined 590 Ma isochrone age (Hashad et al. 1972) and the 570 Ma K-Ar age (SHURMANN 1966) represent the time of emplacement or crustal rebound.

NOWAIR *ET AL.* (1990) mentioned that the Aswan area granites including light gray medium-grained, red coarse-grained and fine-grained varieties are affiliated to post-collisional granites. They also added that these granites are probably formed through progressive differentiation from granodiorite through monzo- to syeno-granite, where they are related to a single magmatic intrusive sequence. They added that the biotite from Aswan granodiorites falls within the metamorphic-metasomatic field of magmatic rocks. However, all of the biotites from Aswan area granites belong to granitic rocks and fall within the Fe^{2+} biotite field.

The present work aims by the combination of HREM, SAED, XRD investigations and electron-microprobe analyses, to declare the structural, mineralogical and chemical variations through the replacement processes of biotite by chlorite in Sohail Island granites, and their implications for elemental behavior through weathering processes.

SAMPLES AND METHODS

Petrographic investigations revealed that; in the Sohail Island granites (Fig.1), biotite associating shreds of primary muscovite occurs in the fine-grained grayish to pinkish granites, while it is accompanied with hornblende in the coarse-grained to pegmatitic varieties located at the north-eastern corner of the island. Biotite frequently occurs as the sole ferromagnesian phase in the medium to coarse-grained red Aswan granite.

Biotite from six representative samples from the Sohail Island granites and chlorite in one of them were subjected to electron-microprobe analyses. The averages of 14 biotite and 2 chlorite analyses are shown in table (1). Electron-microprobe analyses were carried out at the Warsaw University, Poland, with the operating conditions; 15 Kv accelerating voltage and a 15 nA probe current, with a 5 μm spot size and 60-second counting.

$\text{Fe}^{3+} / \text{Fe}^{2+}$ ratios for the Sohail Island biotites and chlorites were estimated through stoichiometric calculations according to Droop (1987) equation.

Biotites in the coarse-grained, hornblende-bearing granites (samples 19 & 23), are generally chloritoidized. They are mostly pleochroic from straw yellow to brown, while some greenish brown varieties can be recorded. Due to alteration processes biotite is disposed by opaques, titanite (sphene) and rutile, where zircon and apatite are enclosed in these biotites (Fig.2). Relatively coarse titanite grains are common all over the rock. Biotite representing the sole mafic mineral in the Aswan granites (sample 1 & 14), is uncommonly chloritoidized with scarce secondary muscovite. In the fine-grained leucogranites (samples 6 & 7), the relatively chloritoidized biotite is associated with fine shreds of primary muscovite (Fig.3).

Generally, no petrographic evidences were noted to indicate that the recorded apatite and zircon inclusions were participated in the biotite-chlorite alteration reactions. It is also worth to mention that, because this biotite is clearly crystallized within plutonic rocks, its microstructures definitely are the result of post-crystallization reactions.

For XRD and TEM studies, biotite grains 0.15-0.35 mm in diameter were separated from 2 samples (23 and 1) by wet sieving, magnetic separation and hand sorting under stereomicroscope. Part of the biotite concentrates was further ground under acetone, where some random samples were picked for XRD investigations. XRD patterns were obtained by

using a PW1830 instrument in the ENMA Labs, equipped with a Co target, operating at 45 Kv and 40 mA.

The TEM investigations were carried out at the Central Labs, Faculty of Science, Menoufiya University, Egypt, on crushed-grain mounts. These mounts were prepared by grinding some of the former biotite separates in an agate mortar and suspending the resultant powder in ethanol before deposition onto a holey carbon grid. Samples were examined by a JEOL, JEM-1320 transmission electron microscope, operating at 100 kv, with an objective lens of spherical aberration coefficient 1.7 mm, and objective aperture of 35 μ m. The data were treated as described by LIVI AND VEBLEN (1987).

RESULTS AND DISCUSSION

CHEMISTRY

The averages of the electron-microprobe analyses and the structural formulae of the investigated biotites and chlorites are given in table (1). The structural formulae of the biotites were calculated on the basis of 22 (O), whereas those of chlorite were calculated on the basis of 36 (O).

The biotites structural formulae show that the 4 co-ordinated (Z-group) elements consist entirely of Si and Al, as they are enough to provide the theoretical 8 atoms in the tetrahedral sites. The number of atoms in the octahedral sites ranges from 3.62 to 5.29, which means that these biotites are of the trioctahedral micas (Y=6) (FOSTER 1960). Potassium constitutes over 95% of the X-site (12 co-ordination) ions in the biotites from the granite samples barren of hornblende. It decreases to about 69% where biotite accompanies hornblende.

Comparison of biotite and chlorite data (Table 1) exhibits a general and apparent increase in MgO and FeO due to the formation of octahedral brucite-like layers in chlorite, which replace the K-layers in biotite and leads to the noted severe decrease in K from biotite to chlorite. A relative decrease in silica is also recorded.

Generally, the major differences in the structural formulae between biotite and its chlorite alteration product, in addition to the remarkable increase in Mg and Fe in chlorite, are the high AlVI content in the chlorite octahedral sites, and the great loss of K and Ti ions from biotite. Ti is inherited in titanite, which is ubiquitously recorded.

It is also worthy to mention that the structures of the two minerals show that the tetrahedral sheets appear to be inherited intact, while there is free element exchange in the octahedral site.

Plotting of the investigated biotites on the classification diagram of DEER *ET AL.* (1966) locates in the biotite field nearby the annite-siderophyllite border (Fig. 4), which is in harmony with WIEWIÓRA (1990) crystallochemical classification of biotite. The affiliation of the present work biotites to the Fe-biotites is confirmed by the plotting on the diagram of FOSTER (1960) (Fig. 5). The plotting of the Sohail Island biotites on the Fe^{3+} - Fe^{2+} - Mg diagram of WONES AND EUGESTER (1965) (Fig.6), suggests that the composition of the biotites are defined by oxygen fugacities close, but slightly higher than the Ni-NiO buffer.

According to the biotite stability diagram of WONES AND EUGESTER (*op. cit.*) (Fig. 7), and as the ratio $100 * (Fe^t / Fe^t + Mg)$ varies from 65% to 73% for the Sohail Island biotites, the formation temperature of these biotites ranges from 710°C to 750°C.

Chlorite after biotite in Sohail hornblende bearing granites with the average formula:

(K 0.12 Na 0.06 Ca 0.04) (Fe²⁺ 2.54 Fe³⁺ 0.54 Al VI 0.79 Mg 1.40 Mn 0.06 Ti 0.04) (Si 3.03 Al_{IV} 0.97) O₁₀ (OH) 8 is the iron-enriched chamosite variety referred by WIEWIÓRA and WEISS (1990).

X-RAY DIFFRACTION

XRD data exhibit the 1M structure type of the biotite (ASTM card No.10-495) and show their association with chlorite and occasionally quartz. The chlorite is represented by the mineral leuchtenbergite (ASTM card No.12-242).

The average cell parameters calculated from the XRD data for the biotite are; $a = 5.36 \text{ \AA}$, $b = 9.24 \text{ \AA}$, $c = 10.23 \text{ \AA}$ and $\beta = 99^\circ 49'$, while those of chlorite are; $a = 5.32 \text{ \AA}$, $b = 9.24 \text{ \AA}$, $c = 14.21 \text{ \AA}$ and $\beta = 97^\circ 08'$. These data can relatively be comparable with those of EGGLETON AND BANFIELD (1985), who referred that the temperature of that hydrothermal alteration is estimated by 338°C (assuming 1 Kb pressure). HECHT ET AL. (1991) on the basis of chlorite solid solution model of WALSH (1986) proposed the 250°C to 300°C to be the alteration temperature of biotite to chlorite. The temperature of Sohail Island chlorite formation

calculated using the equation modified by KRANIDIOTIS AND MACLEAN (1987) after NIEVA (1985) is 272°C.

The average unit cell volume calculated on the basis of XRD data for the biotite is 423.59 Å, whereas that of chlorite is 694.63 Å, referring to the prominence of the alteration mechanism in which 1 biotite is altered to 1 chlorite (mechanism 1 of VEBLEN AND FERRY (1983)). These results can be in harmony with the estimated molar volumes on the basis of the equations proposed by PERRY AND DOWNEY (1982), which are $v = 213.3 - 4.909 [Mg / (Mg + Fe^t + Ti + Mn)]$ for natural chlorite, whereas, $v = 150.6 - 314 [Mg / (Mg + Fe^t + Ti + Mn)]$ for natural biotite. The calculated molar volume of the Sohail Island chlorite is 211.78cm³/mole, whereas it is 150.31cm³/mole for the Sohail Island biotite. These are comparable with the estimated volumes by HELEGSON *ET AL.* (1978) (207.11cm³/mole for clino-chlorite and 149.66cm³/mole for phlogopite).

Nevertheless, petrographic investigations of the studied Sohail Island granites do not show obvious changes in biotite volume through its alteration to chlorite, the fore-mentioned volume changes through the alteration processes of biotite can be re-equilibrated through the existing porosity and the precipitated minerals through the alteration processes, or by the changes in rock volume by the adjustment on fractures (FERROW *ET AL.* 1990).

ELECTRON MICROSCOPY

High-resolution transmission electron microscopy (HRTEM) used in this study, proved to be one of the most effective methods for studying nano-scale intergrowths involving sheet studies. These investigations can introduce structural and compositional high-resolution data about these intergrowths, and to show if they are primary or due to secondary processes.

Generally, the appearance of an HRTEM image is a complex function, not only of the structure being imaged and its orientation but also of the imaging conditions (e.g. lens aberrations and focus conditions) (GUTHRIE AND VEBLEN 1990). However, image interpretation for the Sohail Island biotite and chlorite follows that of VEBLEN (1983) and GUTHRIE AND VEBLEN (*op. cit.*). As in the two fore-mentioned articles and many others in literature, multiple-beam bright-field microscopy was conducted under conditions in which the structural layers of the sheet silicates are imaged as dark fringes, and the interlayer regions appear as white fringes. BANÖS *ET AL.* (1983) referred that bright field HRTEM

images of micas in which the layers are parallel to the electron beam direction generally show dark bands separated by thin bright fringes of 10\AA periodicity.

The HRTEM investigations of the present work biotites reveal that the interfingering of biotite with chlorite visible in the optical microscope extends at all scales down to single layer inter-stratification (Fig.8).

Processes of chloritization can go through two mechanisms portrayed by VEBLEN AND FERRY (1983). Mechanism (1) (Fig.9) is represented by a brucite-like octahedral sheet ($\sim 5\text{\AA}$ thick) appears between two talc-like layers (T-O-T with $\sim 9.3\text{\AA}$ spacing), and the biotite on each side is distorted to make space for the extra brucite. This mechanism requires introduction of substantial material and results in an increase in volume. In mechanism (2), the first indication of alteration is the termination of a single talc-like layer in the biotite followed by edge defects, occasionally with a wedge-shaped gap between the flanking talc-like layers; such defects are presumably the initial focus for alteration. In a following step, the talc-like layer extends its brucite-like octahedral sheet into what has become the interlayer, i.e. a biotite layer has lost its silica tetrahedrons and K-ions and become a brucite-like sheet. This mechanism requires a net removal of material from the biotite and results in a decrease in volume. Thus, two main changes in volume can be recorded; an expansion ($10\text{\AA}\rightarrow 14\text{\AA}$) in mechanism (1), and a contraction ($2\times 10\text{\AA}\rightarrow 14\text{\AA}$) in mechanism (2).

HRTEM micrographs of the Sohail Island chloritized biotite exhibit that mechanism (2) is uncommonly recorded, while mechanism (1) is the ubiquitous (Fig. 10).

KONINGS *ET AL.* (1988) noted that biotite had greater variability in its microstructure and diffraction patterns. The selected area electron diffraction (SAED) patterns of the Sohail Island biotite (Fig. 11), indicate that the basic repeat unit is the 10\AA , with some other superlattice reflections, that refer to the common presence of 1M-biotite type and possibly some other polytypes. That is consistent with the observations of BAILY (1984) that 1M-type is the most common natural biotite polytypes.

The streaking between the dominant spots (Fig. 12) indicates that these polytypes are irregularly inter-layered and/or that these polytypes possess abundant stacking faults (e.g. IJIMA AND ZHU 1982, IJIMA AND BUSECK 1975, KONINGS *ET AL.* 1988, NOE AND VEBLEN 1999).

The biotite-chlorite reaction is commonly accompanied by the formation of micro-precipitates (Fig.13). These micro-precipitates may deform the layers of the investigated sheet silicates and apparently dissolve after complete conversion to chlorite (VEBLEN AND FERRY 1983).

Granular micro-precipitates, reaching up to 20 Å in diameter, are located in the planes of brucite-like layers intercalated in biotite. They may be iron-rich inclusions that can be reported by uncommon powder rings in some SAED, in addition to quartz or amorphous silica, and occasional K-feldspars, similar to the inclusions reported by CHAYES (1955) and FERROW *ET AL.* (1990).

Although the micro-precipitates were not identified rigorously, they are clearly important and an integral part of the alteration reaction in biotite. In areas that have experienced substantial alteration, the micro-precipitates are abundant and can be noticed in the chlorite in the immediate proximity of the partially altered material (Fig.13). However, chlorite farther from biotite and from the partially altered material appears to be barren from these micro-precipitates (VEBLEN AND FERRY 1983).

Mottling in the HRTEM images of the Sohail Island biotites are well pronounced. Type-1 mottling of NOE AND VEBLEN (1999) is well portrayed in the Sohail Island investigated samples (Fig.14). They (*op. cit.*) mentioned that this type of mottling is visible in micrographs that have an end view of the (001) basal plane, and suggested that it results from localized interlayer collapse.

Chemical analyses of phyllosilicates commonly indicate alkali cation concentrations that are less than one atom per formula unit (GUIDOTTI 1984), if the implied vacancies are heterogeneously distributed, then collapsed areas (and mottling) may be an original feature.

Type-2 mottling of NOE AND VEBLEN (*op. cit.*) can also be recorded in the investigated biotites (Fig. 15), which consists of short (few nanometers) curvy lines, which commonly intersect with other lines or terminate. VEBLEN AND FERRY (1983), mentioned that this type of mottling can be correlated with the moiré fringes resulted from interaction of the overlapping layers in different orientations referred by them. They also recorded that the curving of the moiré fringes suggests that the orientation relationships between layers are not exactly identical across the crystal.

CONCLUSION

HRTEM micrographs of the Sohail Island chloritized biotite exhibit that chloritization processes follow mainly mechanism (1) of VEBLEN AND FERRY (1983), where a brucite-like octahedral sheet appears between two talc-like layers. Mechanism (2) is uncommonly recorded, in which a biotite layer lost its silica tetrahedrons and K-ions and become a brucite-like sheet.

SAED patterns of the Sohail Island biotites indicate that the basic repeat unit is the 10 Å, with some other superlattice reflections, referring to the common presence of the 1M-biotite type, and possibly some other polytypes.

The average unit cell volume calculated on the bases of XRD data for biotite is 423.59 Å³, whereas that of chlorite is 694.36 Å³. These values confirm the prominence of the alteration mechanism in which one biotite is altered to one chlorite (1 biotite 10 Å → 1 chlorite 14 Å thick).

The biotite-chlorite reaction is accompanied by the formation of micro-precipitates, which may be iron-rich inclusions, quartz, amorphous silica and K-feldspars.

Mottling recorded in the HRTEM images is represented by the types (1) and (2) of NOE AND VEBLEN (1999). Type (1) probably resulted from localized interlayer collapse, whereas type (2) resulted from intercalation of the overlapping layers in different orientations.

Biotite structural formulae show that they are mostly of the trioctahedral micas (Y=6). Potassium constitutes over 95% of the X sites but decreases to 69% where biotite accompanies hornblende.

The Sohail Island biotite is of the iron-enriched varieties, whereas its chlorite reaction product is represented by the chamosite variety. Their major differences, in addition to the remarkable increase in Fe and Mg in chlorite, are the high AlVI content of chlorite octahedral sites, and the great loss of K and Ti from biotite. Ti is inherited in the recorded titanite. Biotite was probably crystallized between 710°C and 750°C, while the temperature of formation of chlorite is 272°C.

REFERENCES

1. ABDEL-MONEM, A. A. AND HURLEY, P.M. (1980): Age of the Aswan monumental granite, Egypt, by U-Pb dating of zircons. In: Al-Shanti, A.M.S. (ed.), Evolution and mineralization of the Arabian Nubian Shield, New York, Pergamon Press, 3 :141-144.
2. ATTIA, M.I. (1955): Topography, geology and iron-ore deposits of the district east of Aswan, Egypt. Geol. Surv. Egypt, Cairo, 262p.
3. Bailey, S.W. (1984): Classification and structures of micas. Mineral Soc. Amer. Reviews in Mineralogy, 13:1-12.
4. BALL, J. (1907): A description of the first of Aswan cataract of the Nile. Egypt, Surv. Dept., Cairo, 121p.
5. BANFIELD, J.F. AND EGGLETON, R.A. (1988): Transmission electron microscope study of biotite weathering. Clays and clay minerals, 36:47-60.
6. BAÑOS, J.O., AMOURIC, H., DE FOUQUET, C., BARONNET, A. (1983): Interlayering and interlayer slip in biotites as seen by HRTEM. Amer. Miner., 68; 754-758.
7. CHAYES, F. (1955): Potash feldspar as by-product of the biotite-chlorite transformation. J. Geol., 63; 75-82.
8. DEER, W.A., HOWIE, R.A., ZUSSMAN, J. (1966): An introduction to the rock forming minerals. Longman, London, 528p.
9. Droop, G.T.R. (1987): A general equation for estimating Fe³⁺ concentrations in ferromagnesian silicates and oxides from microprobe analyses, using stoichiometric criteria. Mineral. Mag. 51: 431-435.
10. EL-SHAZLY, E.M. (1954): Rocks of Aswan area. Geol. Surv. Egypt, 21p.
11. FERROW, E.A., LONDON, D., GOODMAN, K.S., VEBLEN, AND D.R. (1990): Sheet silicates of the Lawler Peak granite, Arizona: Chemistry, structural variations and exsolution. Contrib. Miner. Petrol., 105:491-501.
12. FERRY, J.M. (1979): Reaction mechanism, physical conditions and mass transfer during hydrothermal alteration of mica and feldspar in granitic rocks from South-Central Main, USA. Contrib. Miner. Petrol., 68; 125-139.
13. FOSTER, M.D. (1960): Interpretation of the composition of tri-octahedral micas. U.S. Geol. Surv. Prof. Pap., 354-B; 11-49.
14. GUIDOTT, C.V. (1984): Micas in metamorphic rocks. Mineralogical Society of American Reviews in Mineralogy, 13:357-468.
15. GUTHRIE, JR., G. D. AND VEBLEN, D.R. (1990): Interpreting one-dimensional high-resolution transmission electron micrographs of sheet silicates by computer simulation. Amer. Miner., 75:276-288.
16. HASHAD, A.H., SAYYAH, T.A., EL-KHOLY, S.B., YOUSSEF, A. (1972): Rb/Sr isotopic age determination of some basement Egyptian granites. Egypt. J. Geol., 16:269-281.
17. HELEGSON, H.C., DELANY, J.M., NESBITT, H.W., BIRD, D.K. (1978): Summary critique of the thermodynamic properties of rock-forming minerals. Amer. J. Sci., 278A:1-229.
18. HECHT, L., SPIEGEL, W., MORTEANI, G. (1991): Multiphase alteration including disseminated uranium mineralization in quartz-depleted granites (episyenites) of Fichtelgebirge, Northern. In: PAGEL AND LEROY (eds), Source Transportation and Deposition of Metals, Balkema, Rotterdam, Bavaria, Germany: 53-56.
19. HUME, W.F. (1935): Geology of Egypt, V.II, Part II. The later plutonic and minor intrusive rocks. Survey of Egypt, Cairo, 301-688.
20. HUNTING GEOLOGY AND GEOPHYSICS LTD. (1967): Assessment of the mineral potential of Aswan region, U.A.R. UNDP and regional planning of Aswan, 138p.
21. IJIMA S. AND BUSECK, P.R. (1978): Experimental study of disordered mica structure by HRTEM. Acta Crystallographica, 34A:709-719.
22. IJIMA, S. AND ZHU, J. (1982): Electron microscopy of a muscovite-biotite interface. Amer. Miner., 67:1195-1205.
23. KALINOWSKI, B.E. AND SCHWEDA, P. (1996): Kinetics of muscovite, phlogopite and biotite dissolution and alteration at pH 1-4, room temperature. Geochemica Cosmochemica Acta, 60:367-386.
24. KONINGS, R.J.M., BOLAND, J.N., VRIED, S.P., JANSON, J.B.H. (1988): Chemistry of biotites and muscovites in Abas granites, northern Portugal. Amer. Miner., 73:754-765.
25. LITTLE, O.H. AND ATTIA, M.I. (1943): The development of the Aswan district, with notes on the minerals of South-Eastern Egypt. Geol. Surv. Egypt, Cairo, 107p.

26. LIVI, K.J.T. AND VEBLER, D. R. (1987): "Estonite" from Easton, Pennsylvania: A mixture of phlogopite and a new form of serpentine. *Amer. Miner.*, 72:113-125.
27. NOE, D.C. AND VEBLER, D.R. (1999): HRTEM analysis of dislocation cores and stacking faults in naturally deformed biotite crystals. *Amer. Miner.*, 84:1925-1931.
28. NOWAIR, A.M., ABU EL ELA, A.M., SEWIFI, B.M. (1990): New contributions to the geology, geochemistry and tectonic setting of the Aswan granites, southern Egypt. *Qatar Univ. Sci. Bull.*, 10:395-419.
29. PARRY, W.T. AND DOWNEY, L.M. (1982): Geochemistry of hydrothermal chlorite replacing igneous biotite. *Clays and Clay Mineralogy*, 30(2):81-90.
30. SHURMANN. H.M.E., 1966; *The Pre-Cambrian along the Gulf of Sues northern part of Red Sea*. Leiden, E. J. Brill, 404p.
31. SPEER, J.A. (1984): Micas in igneous rocks. *Mineral Soc. Am. Reviews in Mineralogy*, 13:299-365.
32. VEBLER, D.R. (1983): Microstructures and mixed layering in inter-grown wonesite, chlorite, talc, biotite and kaolinite. *Amer. Miner.*, 68:566-580.
33. VEBLER, D.R. AND FERRY, J.M. (1983): A TEM study of the biotite-chlorite reaction and comparison with petrologic observations. *Amer. Miner.*, 68:1160-1168.
34. WONES, D.R. AND EUGESTER, H.P. (1965): Stability of biotite, experimental, theory and application. *Amer. Miner.*, 50:1228-1272.
35. WALSH, J.L. (1986): A six-component chlorite solid solution model and the conditions of chlorite formation in hydrothermal and geothermal systems. *Economic Geology*, 81:631-703.
36. ZEN E-AN (1988): Phase relations of peraluminous granitic rocks and their petrogenetic implications. *Ann. Rev. Earth Planet Sci.*, 16:21-51.



Table.1. Averages of microprobe analyses and structural formulae of biotite and chlorite from the Sohail Island granites.

SAMPLE NO.	BIOTITE						CHLORITE
	23 (4)	19 (1)	1 (1)	14 (1)	6 (3)	7 (4)	19 (2)
SiO ₂	34.855	35.60	34.153	36.04	35.50	35.575	27.73
TiO ₂	2.779	2.68	4.326	3.54	2.12	3.547	0.54
Al ₂ O ₃	14.620	13.98	14.676	14.87	15.82	15.575	15.11
Cr ₂ O ₃	0.042	0.01	0.025	0.30	B.d.	0.005	B.d.
FeO	24.14	23.59	22.038	20.93	21.89	23.139	27.80
Fe ₂ O ₃	4.798	4.83	5.169	5.23	4.22	4.971	6.52
MnO	0.387	0.48	0.342	0.79	0.53	0.492	0.62
MgO	5.995	5.72	5.724	5.78	6.76	6.679	8.62
BaO	0.005	0.02	B.d.	B.d.	0.003	B.d.	B.d.
CaO	B.d.	B.d.	B.d.	B.d.	B.d.	B.d.	0.37
Na ₂ O	0.271	0.20	0.221	0.11	.21	0.231	0.20
K ₂ O	9.045	9.49	9.590	9.69	9.84	9.581	0.94
TOTAL	96.94	96.60	96.26	97.28	96.94	97.80	88.45
Si	5.202	5.327	5.115	5.291	5.239	5.211	6.058
Al ^{IV}	2.570	2.464	2.589	2.271	2.738	2.687	1.942
Al ^{VI}	0.000	0.000	0.000	0.000	0.011	0.000	1.946
Ti	0.312	0.302	0.487	0.391	0.235	0.281	0.089
Fe ₃	0.538	0.543	0.582	0.577	0.468	0.547	1.071
Fe ₂	3.013	2.952	2.760	2.570	2.702	2.712	5.081
Cr	0.005	0.001	0.003	0.035	0.003	0.001	0.000
Mn	0.049	0.061	0.043	0.098	0.066	0.061	0.115
Mg	1.334	1.276	1.278	1.265	1.492	1.458	2.808
Ba	0.000	0.001	0.000	0.000	0.001	0.000	0.000
Ca	0.000	0.000	0.000	0.000	0.000	0.000	0.086
Na	0.078	0.058	0.064	0.031	0.059	0.066	0.086
K	1.722	1.812	1.832	1.815	1.825	1.790	0.230
CATIONS	14.823	14.86	14.753	13.403	14.797	14.814	19.540
O	22	22	22	22	22	22	36
Fe_FeMg	0.69	0.70	0.68	0.67	0.64	0.65	0.65
Mg_FeMg	0.31	0.30	0.32	0.33	0.36.	0.35	0.36

B.d.: Below detection

FIGURES CAPTIONS

Fig. 1. Geologic map of Aswan area. Map after Attia (1955).

Fig. 2. Photomicrograph of a thin section show in chloritized biotite in sample 23. C.N, X=95

Fig. 3. Photomicrograph of a thin section showing biotite in sample 23. C.N., X=74.

Fig. 4. Composition of Sohail Island biotites in terms of Fet/ (Fet+Mg) and Al.

The classification is after DEER *ET AL.* (1966).

Fig.5. Ternary diagram exhibiting the relation between the octahedral cations of Sohail Island biotites. The fields after FOSTER (1960).

Fig.6. $Fe^{3+} - Fe^{2+} - Mg$ ternary diagram of Sohail Biotites. The fields in the diagram after WONS AND EUGESTER (1965).

Fig.7. Biotite stability diagram of specific [Fet/(Fet+Mg)] values as a function of oxygen fugacity and temperature at 2070 bars total pressure. The curves and fields after WONES AND EUGESTER (1965). Heavily shaded area represent the studied biotites.

Fig.8. HRTEM image of biotite showing the chloritization of the investigated biotites.

Fig.9. Schematic representation of the two different mechanisms for forming a single layer of chlorite in biotite, proposed by VEBLEN AND FERRY (1983).

Fig.10. HRTEM image of Sohail Island biotite showing bructization processes of Biotite, through its alteration to chlorite, according to the two mechanisms of VEBLEN AND FERRY (1983).

Fig.11. The selected-area electron diffraction (SAED) of Sohail island biotite showing streaking parallel to c^* in rows caused by the random spacing.

Fig.12. The selected-area electron diffraction (SAED) of Sohail island biotite showing spots of 1M-biotite polytype, with extra spots of some other polytypes and probably chlorite.

Fig.13. HRTEM image showing the micro-precipitates distributed in Sohail Island chloritized biotites. Notice that the highly chloritized areas are free from precipitates.

Fig. 14. HRTEM image showing (Type 1) mottling in Sohail Island biotite.

Fig. 15. HRTEM image showing (Type 2) mottling in Sohail Island biotite.

LEGEND

- ◀ Biotites from coarse-grained to pegmatitic granite.
- ◆__ Biotites from Aswan granite.
- ▼__ Biotites from fine-grained, two-mica granite.

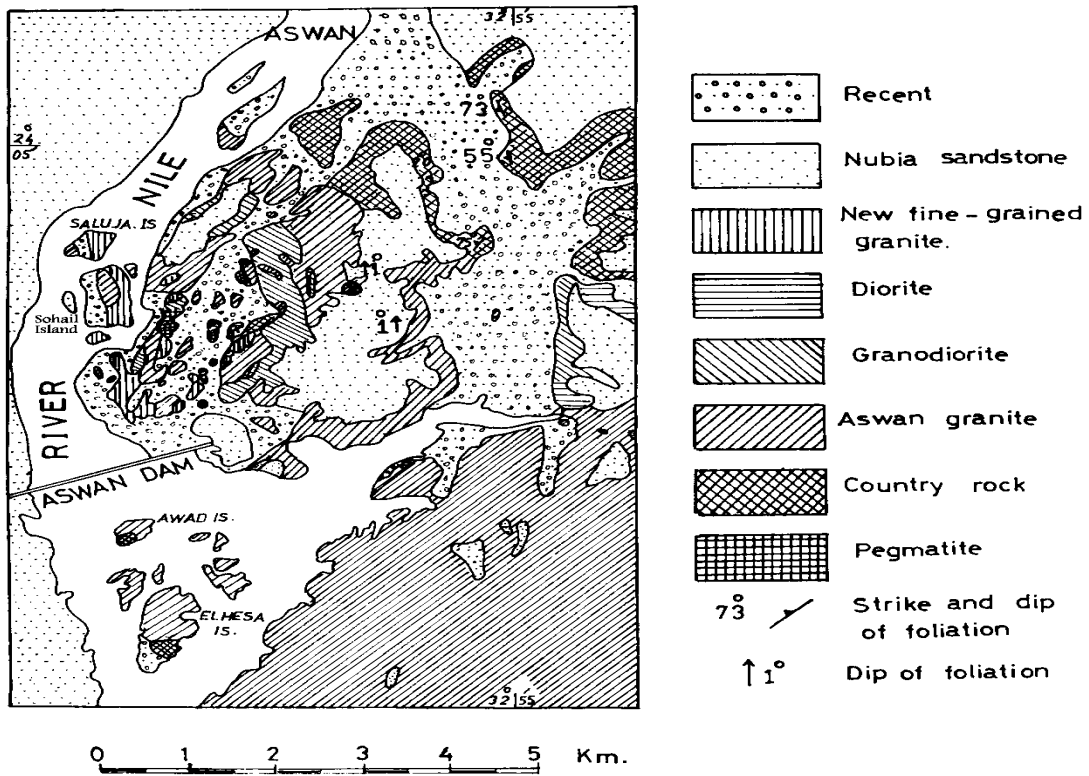


Fig. 1. Geologic map of Aswan area. Map after Attia (1955).

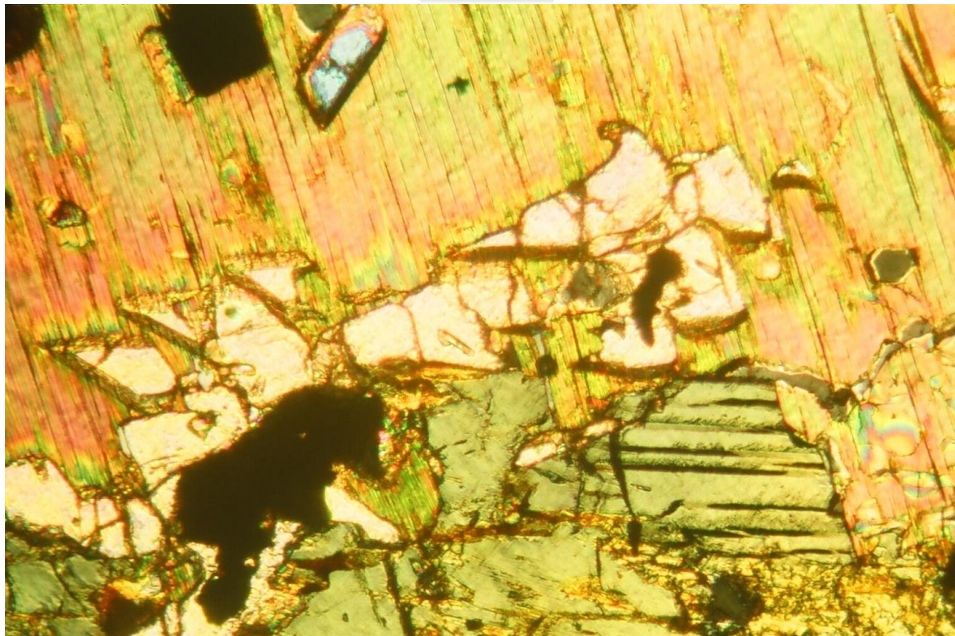


Fig. 2: Photomicrograph of a thin section for chloritized biotite associating hornblende in sample 23, C.N., X=95.

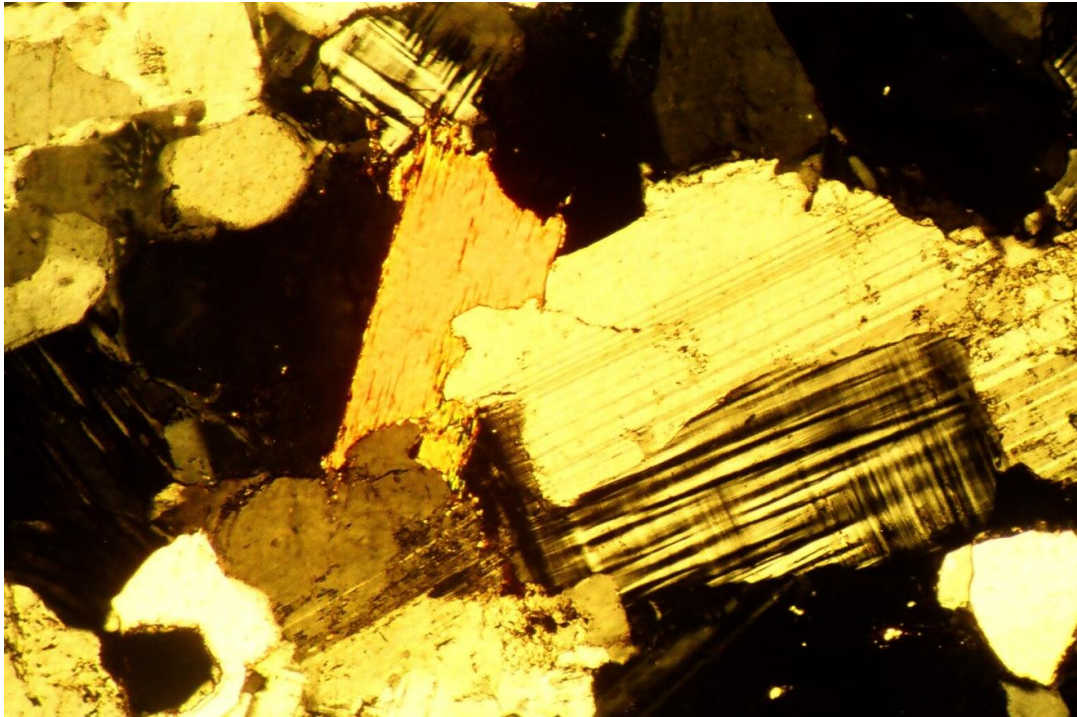


Fig. 3: Photomicrograph of a thin section showing biotite in sample 14, C.N., X=95.

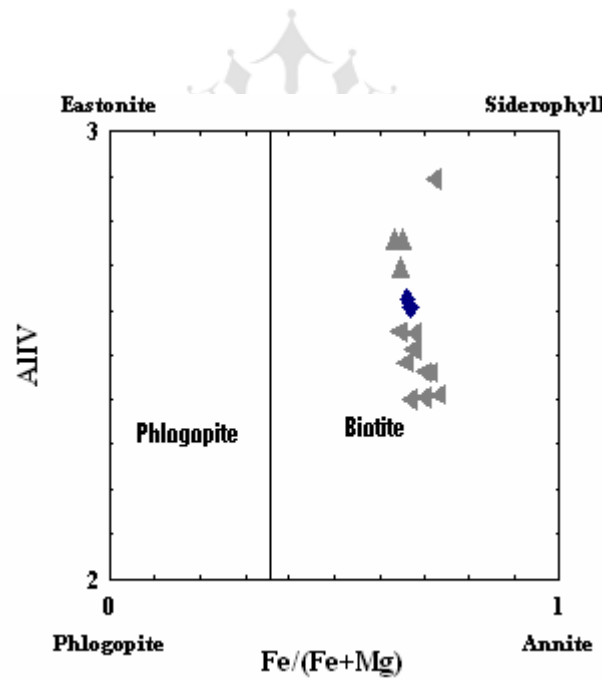


Fig. 4. Composition of Sohail Island biotites in terms of $Fe/(Fe+Mg)$ and Al_{IV} . The classification is after DEER *ET AL.* (1966).

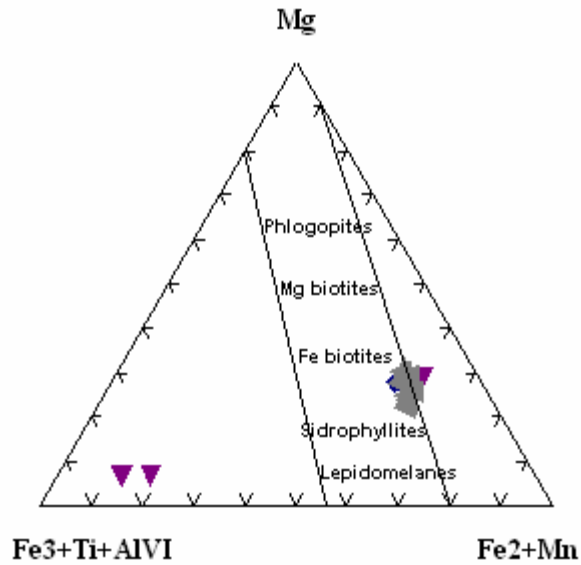


Fig. 5. Ternary diagram exhibiting the relation between the octahedral cations of Sohail Island Biotites. The fields after FOSTER (1960).

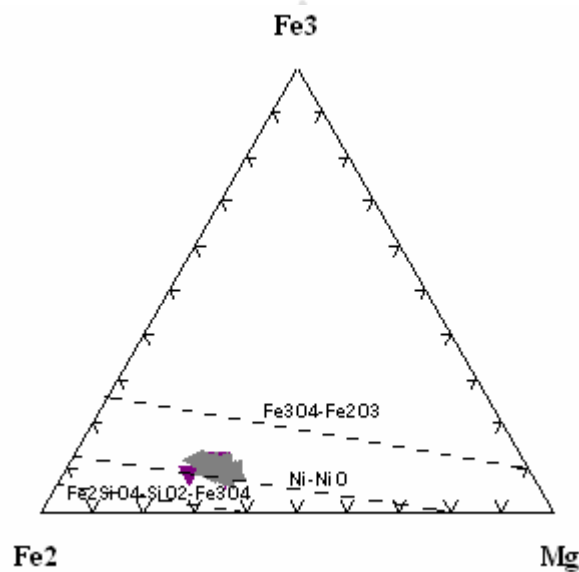


Fig. 6. Fe₃ – Fe₂ – Mg ternary diagram of Sohail Biotites. The fields in the diagram after WONS AND EUGESTER (1965).

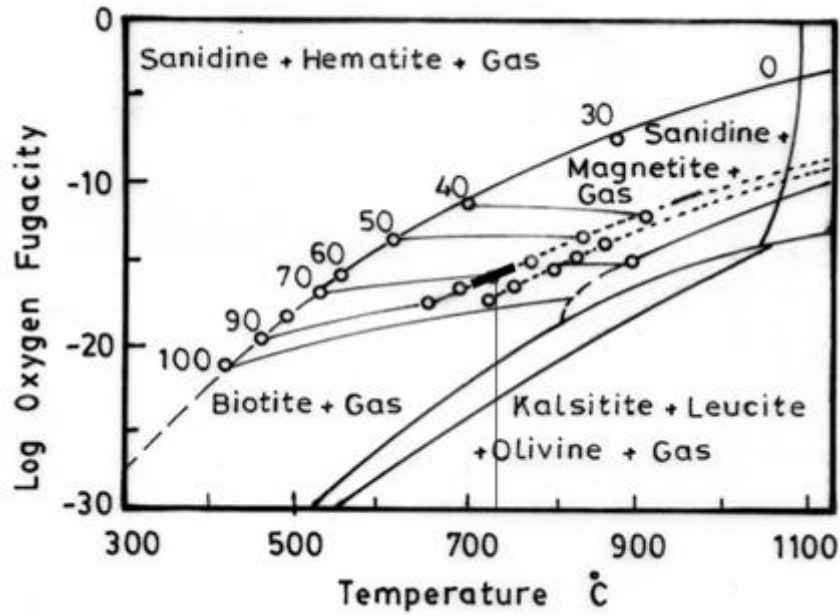


Fig 7. Biotite stability diagram of specific $[Fe^{2+}/(Fe^{2+}+Mg)]$ values as a function of oxygen fugacity and temperature at 2070 bars total pressure. The curves and fields after WONES AND EUGESTER (1965). Heavily shaded area represent the studied biotites.

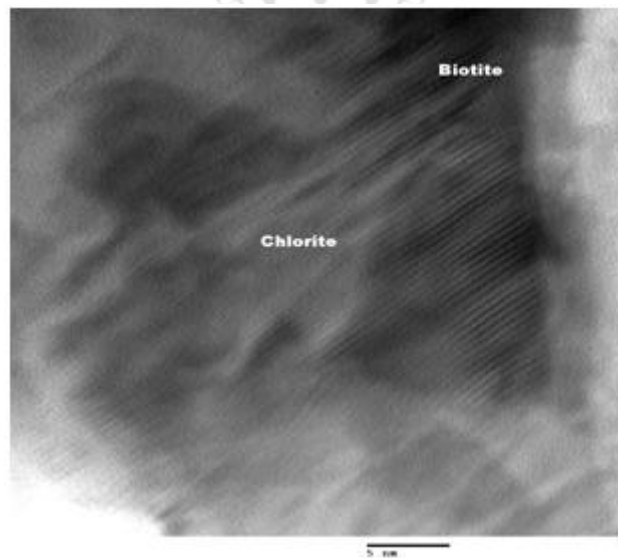


Fig. 8. HRTEM image of biotite showing the chloritization of the investigated biotites.

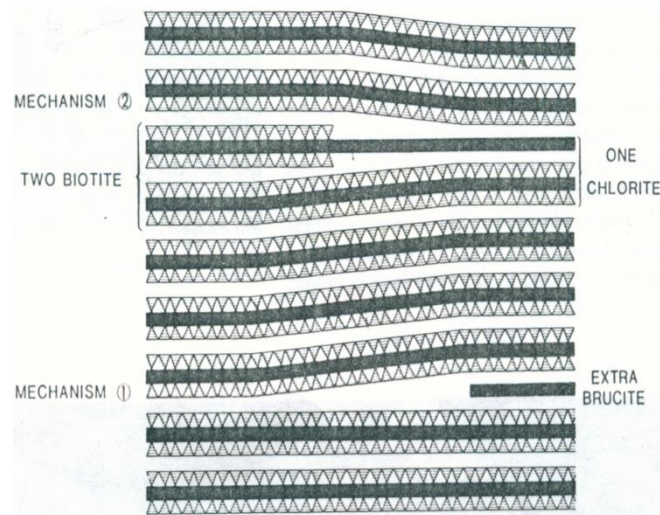


Fig 9. Schematic representation of the two different mechanisms for forming a single layer of chlorite in biotite, proposed by VEBLEN FERRY (1983).

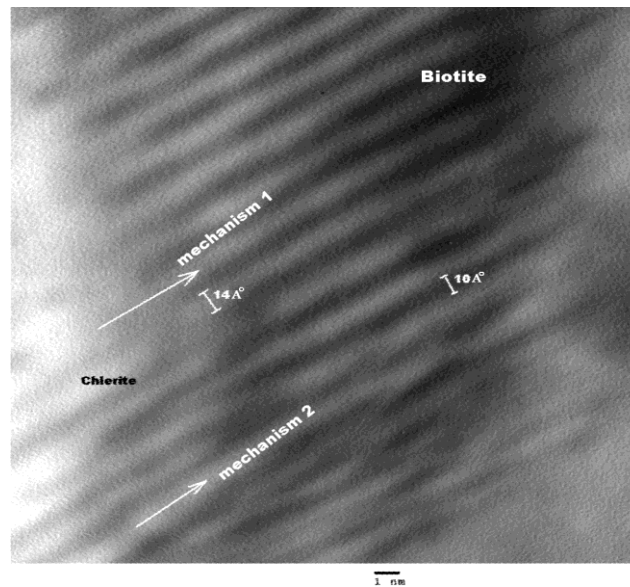


Fig. 10. HRTEM image of Sohail Island biotite showing brucitization processes of biotite, through its alteration to chlorite, according to the two mechanisms of VEBLEN AND FERRY (1983).



Fig. 11. The selected-area electron diffraction (SAED) of Sohail island biotite showing streaking parallel to c^* in rows caused by the random spacing.

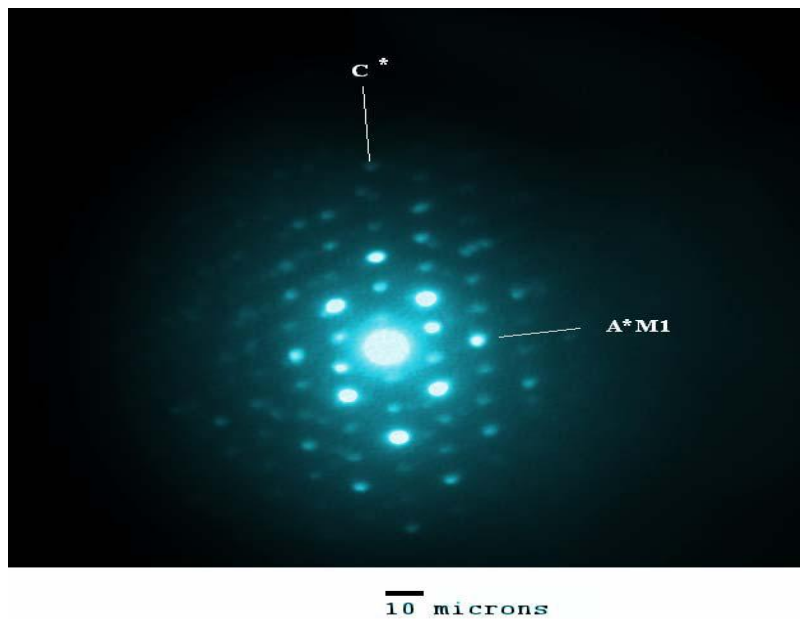


Fig. 12. The selected-area electron diffraction (SAED) of Sohail island biotite showing spots of 1M-biotite polytype, with extra spots of some other polytypes and probably chlorite.

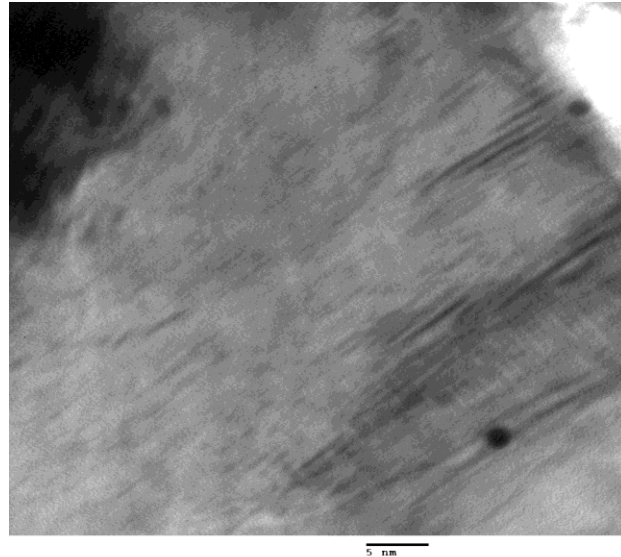


Fig. 13. HRTEM image showing the micro-precipitates distributed in Sohail Island chloritized biotites. Notice that the highly chloritized areas are free from precipitates.

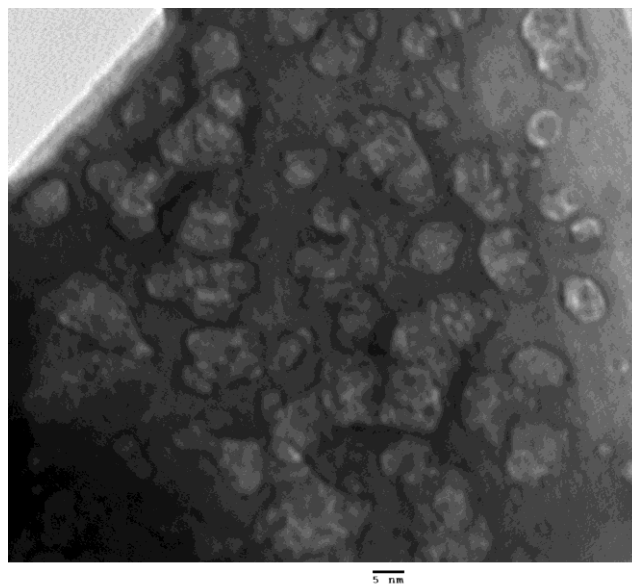


Fig. 14. HRTEM image showing (Type 1) mottling in Sohail Island biotite.

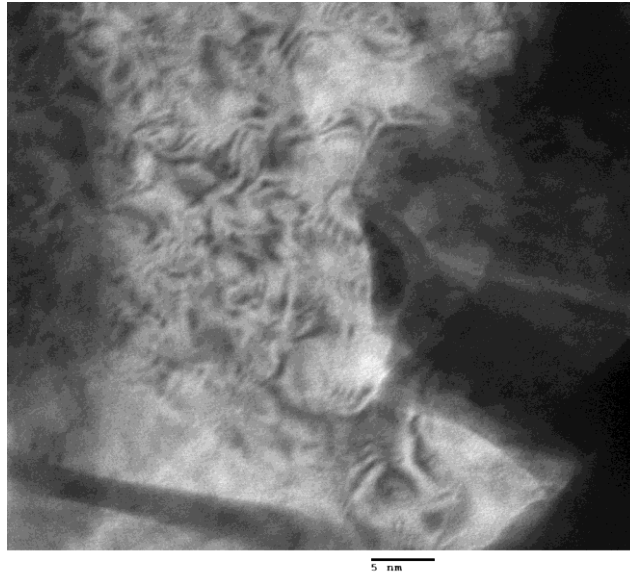


Fig. 15. HRTEM image showing (Type 2) mottling in Sohail Island biotite.

